Journal of Energy Chemistry 55 (2021) 444–448

Contents lists available at ScienceDirect

Journal of Energy Chemistry

journal homepage: www.elsevier.com/locate/jechem

http://www.journals.elsevier.com/journal-of-energy-chemistry/

Metal-seed assistant photodeposition of platinum over Ta_3N_5 photocatalyst for promoted solar hydrogen production under visible light

Juhong Lian [a,b], Deng Li [b], Yu Qi [b], Nengcong Yang [b], Rui Zhang [c], Tengfeng Xie [c], Naijia Guan [a], Landong Li [a], Fuxiang Zhang [b,*]

[a] School of Materials Science and Engineering, National Institute for Advanced Materials, Nankai University, Tianjin 300350, China
[b] State Key Laboratory of Catalysis, iChEM, Dalian Institute of Chemical Physics, Chinese Academy of Sciences, Dalian National Laboratory for Clean Energy, Dalian 116023, Liaoning, China
[c] College of Chemistry, Jilin University, Changchun 130012, Jilin, China

ARTICLE INFO

Article history:
Received 13 June 2020
Revised 7 July 2020
Accepted 7 July 2020
Available online 19 July 2020

Keywords:
Tantalum nitride
Cocatalyst
Charge separation
Contact interface
Metal-seed assistant photodeposition
Solar hydrogen production

ABSTRACT

Cocatalysts play a vital role in accelerating the reaction kinetics and improving the charge separation of photocatalysts for solar hydrogen production. The promotion of the photocatalytic activity largely relies on the loading approach of the cocatalysts. Herein, we introduce a metal-seed assistant photodeposition approach to load the hydrogen evolution cocatalyst of platinum onto the surface of Ta_3N_5 photocatalyst, which exhibits about 3.6 times of higher photocatalytic proton reduction activity with respect to the corresponding impregnation or photodeposition loading. Based on our characterizations, the increscent contact area of the cocatalyst/semiconductor interface with metal-seed assistant photodeposition method is proposed to be responsible for the promoted charge separation as well as enhanced photocatalytic H_2 evolution activity. It is interesting to note that this innovative deposition strategy can be easily extended to loading of platinum cocatalyst with other noble or non-noble metal seeds for promoted activities, demonstrating its good generality. Our work may provide an alternative way of depositing cocatalyst for better photocatalytic performances.

In view of the conventional fossil fuel shortage and related environmental issues, the development of clean and renewable energy sources has become significantly important [1]. Given that solar energy and water are naturally abundant, photocatalytic water splitting thus provides an attractive approach to directly convert and store solar energy into clean and renewable hydrogen [2,3]. The photocatalyst usually composes of a light-absorbing semiconductor and a cocatalyst, where the cocatalyst facilitates the charge separation and accelerates the surface reaction kinetics [4]. Besides the catalytic ability of the cocatalyst itself, the charge separation and transfer at the interface of cocatalyst/semiconductor are also important for the photocatalytic performance, which are mostly determined by the quality of interface including the intimateness and the interfacial contact area [5,6]. Accordingly, development of novel strategy to address the improvement of the interface charge separation has inspired continuous interest.

It has been demonstrated that the interface contact area and compactness between cocatalyst/semiconductor are extremely important for the interface charge separation [7–9]. Conventionally, the cocatalysts have been widely loaded on the surface of semiconductors by using as-prepared cocatalyst particles (mix-adsorption method) or cocatalyst precursors (photodeposition, impregnation or other in-situ growing methods) [10–13]. The former approach usually encounters a large charge transfer resistance at the interface caused by the weak physical connection between the cocatalyst and semiconductor [14]. Comparatively, much stronger interaction between photocatalyst and cocatalyst can be achieved by the latter, among which impregnation (Imp) and photodeposition (PD) methods have been mostly adopted due to the low-cost and convenient features [15–23]. Compared to the PD method, the Imp method could make a much stronger interface interaction because of the calcination process at a certain higher temperature, while which simultaneously causes the aggregation of nanoparticles leading to the decreased interface contact areas. In this case, the strong interface interaction and homogeneous

* Corresponding author.
E-mail address: fxzhang@dicp.ac.cn (F. Zhang).

https://doi.org/10.1016/j.jechem.2020.07.034
2095-4956/

dispersion of the deposited cocatalyst cannot be obtained simultaneously by the single PD or Imp method. Accordingly, it is highly desirable to develop innovative method to combine the advantages of both PD and Imp for homogeneous dispersion and strong interface interaction respectively.

Herein we introduce an innovative metal-seed assistant photodeposition approach that combines the advantage of single Imp and PD method. Specifically, Ta_3N_5, one of the most popular visible-light-responsive photocatalysts [24–28], was employed as the model photocatalyst, and the platinum was deposited as the cocatalyst. The deposition of platinum cocatalyst consists of two steps: One is the deposition of platinum seed on the surface of Ta_3N_5 by the conventional impregnation method, and the other is the photodeposition. The first seed planation by the impregnation route is expected to make a strong interface interaction but free of aggregation because of the low content of platinum used. As seen in the Fig. S1(a), although the impregnated metallic platinum seed cannot be seen after H_2 flow reduction because of the low content, the existence of Pt seed (0.0093 wt%) can be proved by the inductively coupled plasma atomic emission spectroscopy (ICP-AES). The impregnated Pt seed can be expected to trap the photogenerated electrons for photoreduction deposition of further platinum. (Fig. S1b). It means that in this case, the initial impregnated platinum acts as the metal seed for the extensional growth of platinum by photodeposition. It should be pointed out that in order to remove the influence of surface wettability, all the surface of the Ta_3N_5 photocatalyst was modified by magnesia according to our previous method [6]. And as a comparative illustration, the platinum cocatalyst on the surface of Ta_3N_5 photocatalyst was also deposited by single impregnation and photodeposition respectively. The as-synthesized three kinds of samples were correspondingly denoted as Pt(Imp)/Ta_3N_5, Pt(PD)/Ta_3N_5 and Pt(Imp-PD)/Ta_3N_5 respectively. On the basis of detailed experimental and characterized results, it reveals that the photocatalytic H_2 evolution rate on the Pt(Imp-PD)/Ta_3N_5 sample is obviously superior to that of Pt(Imp)/Ta_3N_5 or Pt(PD)/Ta_3N_5, as should result from the improved interface charge separation. As an extended illustration, other metal seeds or semiconductor photocatalysts were further investigated to be similarly feasible, demonstrating the generality of our innovative strategy.

The photocatalytic H_2 evolution activities of the three typical samples were evaluated in the methanol aqueous solution under visible light irradiation. Firstly, the effect of Pt seed and photodeposition Pt amounts on the H_2 evolution rate for Pt(Imp-PD)/Ta_3N_5 sample was optimized and given in Fig. S2. Based on the optimized results, the amounts of Pt seed and photodeposition Pt were fixed at 0.01 wt% and 1.0 wt%, respectively. For compared discussion, the amounts of Pt in Pt(Imp)/Ta_3N_5 and Pt(PD)/Ta_3N_5 samples were also fixed at 1.0 wt%. It should be noted that the pristine Ta_3N_5 without Pt cocatalyst performs no H_2 production activity under visible light irradiation, while the three typical photocatalysts continuously produce H_2 in the experimental region after loading of Pt cocatalysts (Fig. 1a). It is interesting to see that the Pt(Imp-PD)/Ta_3N_5 shows a much higher activity with respect to the Pt(Imp)/Ta_3N_5 or Pt(PD)/Ta_3N_5 samples. The actual loading amounts of Pt on the Pt(Imp)/Ta_3N_5, Pt(PD)/Ta_3N_5 and Pt(Imp-PD)/Ta_3N_5 samples were evaluated by the inductively coupled plasma atomic emission spectroscopy (ICP-AES) to be 1.0 wt%, 0.76 wt% and 0.82 wt%, respectively (Fig. 1b). As an extended discussion, the photocatalytic H_2 evolution rate is thus normalized by the Pt content loaded. As seen in Fig. 1(c), the activity on the Pt(Imp-PD)/Ta_3N_5 (5.44 mmol/(h·g Pt)) still remains ca. 3.4 times of higher than that of Pt(Imp)/Ta_3N_5 and Pt(PD)/Ta_3N_5 (1.58 and 1.6 mmol/(h g Pt)), demonstrating the superiority of our metal-seed assistant photodeposition approach in promoting the photocatalytic proton reduction reaction.

In order to get insight into the enhanced photocatalytic performance, we characterized the three typical samples in detail. First of all, the morphology and distribution of the deposited Pt cocatalysts were analyzed by the high-resolution scanning electron microscope (HRSEM). As shown in the HRSEM images (Fig. S3), the surface of the prepared Ta_3N_5 is clean and smooth. After loading of Pt cocatalysts, distinct Pt particles can be observed on the surface of Ta_3N_5 by the different methods (Fig. 2a–c). Specifically, the Pt particles on the Pt(Imp)/Ta_3N_5 sample are of spherical morphology with particle sizes grow largely after calcination (Fig. 2a). Fig. S4 (a) shows that the average particle size of Pt on the Pt(Imp)/Ta_3N_5 sample is ca. 4.1 nm, which is larger than that obtained by the PD approach (2.2 nm). The enlarged particle size will lead to decrease of surface active sites. The surface active sites of Pt cocatalysts in the three typical samples were characterized by the CO chemical absorption experiment with results given in Table S1, in which the Pt(Imp)/Ta_3N_5 shows the lowest surface active sites because of its largest Pt particle size. The Pt particles in Pt(PD)/Ta_3N_5 sample are the smallest (Fig. 2b and S4b), showing the strongest light shading effect on Ta_3N_5 (Fig. S5). Interestingly, the Pt particles in Pt(Imp-PD)/Ta_3N_5 seem to grow along the edge of Ta_3N_5 and exhibit a highly dispersive worm-like morphology (Fig. 2c), which is expected to create increased contact area between Pt cocatalyst and Ta_3N_5 photocatalyst for promoted charge transfer. The increscent interfacial contact area between Pt cocatalyst and Ta_3N_5 photocatalyst can be further confirmed by HRTEM image given in Fig. 2(f). All the deposited Pt cocatalysts in the three typical samples are intimately contacted with the Ta_3N_5 (Fig. 2d–f).

The crystal structures of the three typical samples examined by X-ray diffraction (XRD) measurement are almost identical as the

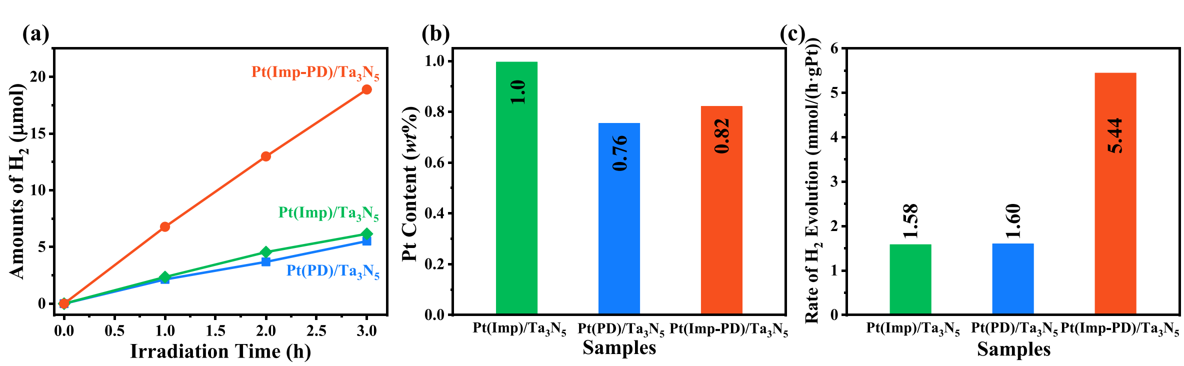

Fig. 1. Comparison of the three typical samples: (a) Time course curves of the photocatalytic H_2 evolution; (b) the loaded Pt amount analyzed by the inductively coupled plasma atomic emission spectroscopy (ICP-AES); (c) rates of H_2 evolution normalized by the amount of loaded Pt (g).

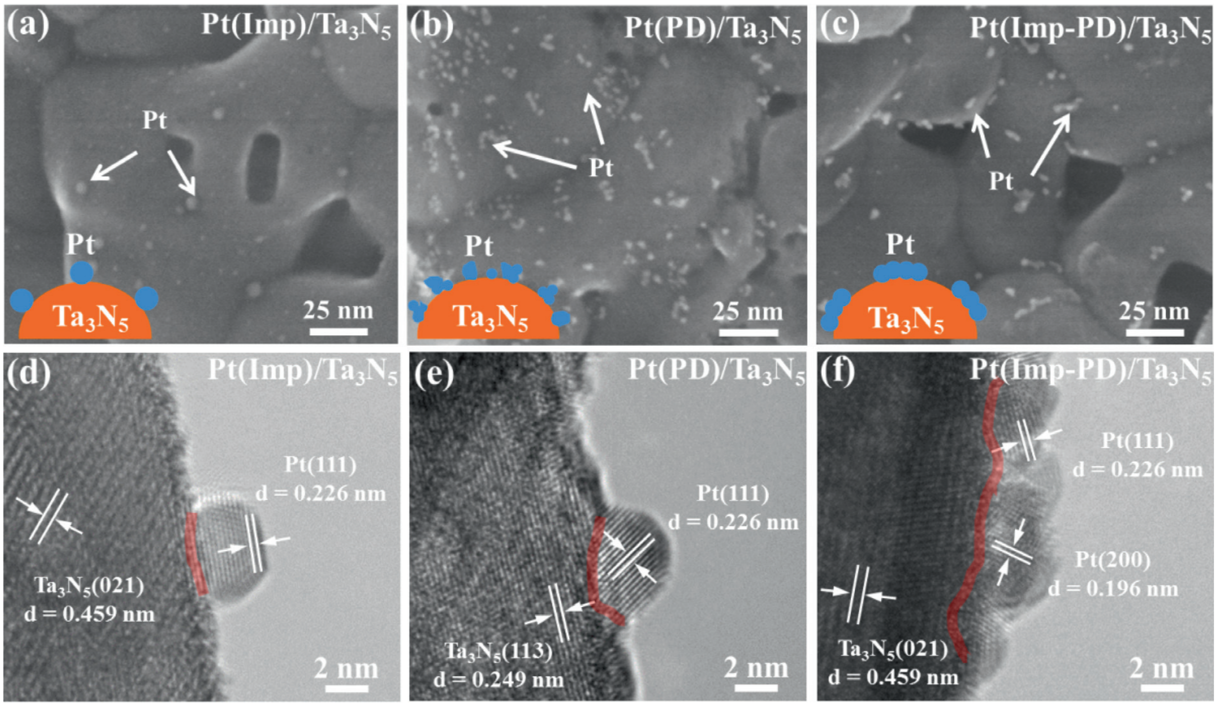

Fig. 2. High-resolution SEM images of (a) Pt(Imp)/Ta_3N_5, (b) Pt(PD)/Ta_3N_5 and (c) Pt(Imp-PD)/Ta_3N_5. The inserted diagrams in Fig. 2(a-c) represent the morphology and distribution of Pt particles with the three different methods. High-resolution TEM images of (d) Pt(Imp)/Ta_3N_5, (e) Pt(PD)/Ta_3N_5 and (f) Pt(Imp-PD)/Ta_3N_5. The red transparent line in the HRTEM images refers to the contact interface between the loaded Pt cocatalyst and the Ta_3N_5 photocatalyst.

pristine Ta_3N_5 photocatalyst (Fig. S6), indicating the crystal structure of the Ta_3N_5 is not obviously altered during the deposition of Pt cocatalysts. No obvious diffraction peaks assigned to Pt can be observed due to the low loading amount. However, the existence of Pt on the Ta_3N_5 surface can be evidenced by the X-ray photoelectron spectroscopy (XPS, Fig. 3). The Pt 4*f* peaks in the three samples are fitted into two couples of peaks, which can be assigned to metallic Pt^0 and Pt^{2+} with adsorbed oxygen (Pt-O_{ads} species) respectively [29]. Notably, the Pt $4f_{7/2}$ peak ascribed to Pt^0 is

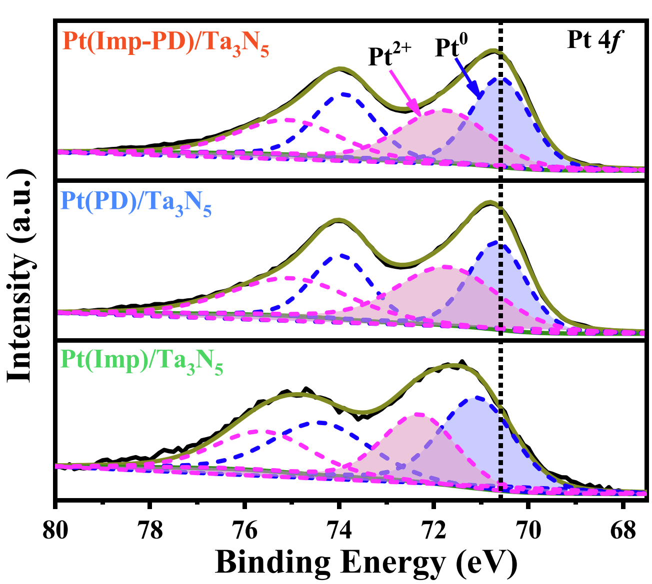

Fig. 3. Pt *4f* XPS spectra of Pt(Imp)/Ta_3N_5, Pt(PD)/Ta_3N_5 and Pt(Imp-PD)/Ta_3N_5 samples. The insert vertical line in the XPS spectra labels the peak position of the Pt^0 spectra.

shifted from 71.1 eV for Pt(Imp)/Ta_3N_5 to 70.7 and 70.6 eV for Pt (PD)/Ta_3N_5 and Pt(Imp-PD)/Ta_3N_5 respectively, demonstrating the loaded Pt species through PD process in the Pt(PD)/Ta_3N_5 and Pt (Imp-PD)/Ta_3N_5 samples should be more electron-sufficient than that Pt(Imp)/Ta_3N_5.

Normally, the activity of one photocatalyst is integrally determined by the efficiencies of light absorption, charge separation and surface catalysis [8]. As demonstrated by results of the XRD patterns and UV–Vis spectra, the differences of crystallization and light absorption on the three typical samples are minor, the efficiency of light absorption on them should be similar. Additionally, the content and active surface area of loaded platinum are close, so the similar surface catalysis can be also expected. Accordingly, the remarkably promoted H_2 evolution rate is proposed to result from the improvement of charge separation. To confirm it, the charge separation of the three samples was thus characterized by the difference of open circuit voltage (ΔOCV) under light and dark conditions, surface photovoltage (SPV) spectra and time-resolved photoluminescence (TRPL) spectra. Basically, the separation of photogenerated charges on photocatalysts under irradiation will lead to change of surface voltage on the photocatalyst, so the surface voltage change before and after irradiation can be used as an indicator of the charge separation on the photocatalytic system [30–32]. As shown in Fig. 4(a and b), the Pt(Imp-PD)/Ta_3N_5 exhibits much larger surface photo-induced voltage with respect to Pt(Imp)/Ta_3N_5 or Pt(PD)/Ta_3N_5 sample, indicating more efficient separation of photo-generated electrons from Ta_3N_5 photocatalyst to the Pt cocatalyst. It is worth noting that no surface photovoltage will be generated for all the samples when the wavelength is beyond absorption edge of Ta_3N_5 in Fig. 4(b) (600 nm, see the UV–vis spectra in Fig. S5). The single Ta_3N_5 shows the minimum surface photovoltage value, while the surface photo-voltage values increase after loading of Pt cocatalysts, even for the sample with the low content of Pt seed loading (Pt(seed)/Ta_3N_5). Importantly, the values of the surface photo-voltage of the three typical samples

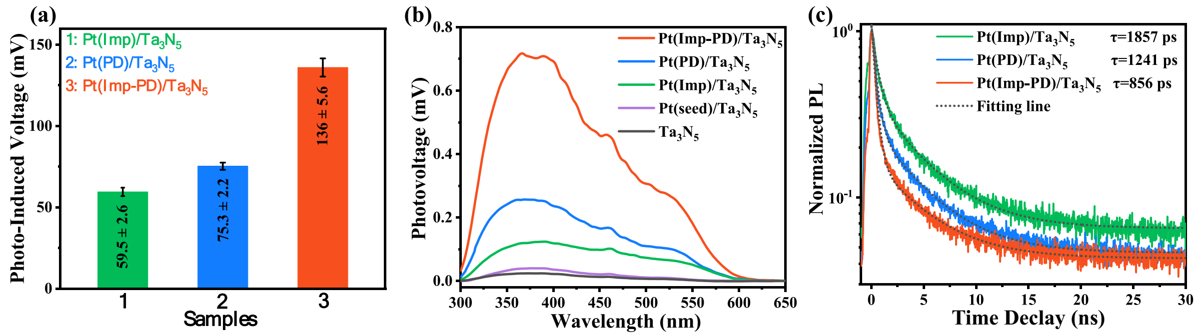

Fig. 4. Photogenerated charge separation characterization of Pt(Imp)/Ta_3N_5, Pt(PD)/Ta_3N_5 and Pt(Imp-PD)/Ta_3N_5 three typical samples: (a) Difference of open circuit voltage (ΔOCV) under light and dark conditions, 300 W Xe lamp ($\lambda \geq 420$ nm); (b) surface photovoltage (SPV) spectra, Experimental conditions: $\lambda_{irradiation}$ from 300 nm to 800 nm with a 500 W Xe lamp; (c) PL decay spectra collected at the indicated emission wavelengths 595 nm under an excitation at 405 nm. The dotted lines are the fits of the kinetics to a biexponential function with the average lifetimes τ.

increased by an order of magnitude compared with Ta_3N_5. The charge separation property was further evidenced by the time-resolved photoluminescence (TRPL) spectra (Fig. 4c) with the PL decays fitted by a biexponential function (Table S2), based on which the PL decay lifetime on the three samples is in a good according with their activity order.

Based on the above results, a short summary can be made that the light absorption and surface catalysis of the three samples have little influence on the photocatalytic activity, while the improved charge separation mainly contributes to the superior photocatalytic H_2 evolution activity of Pt(Imp-PD)/Ta_3N_5 sample. Our metal-seed assistant photodeposition method was based on the speculation that the first metal seed planation by the impregnation route can make a strong interface interaction and easily collect the photogenerated electrons for further photoreduction of platinum precursor. In this case, the amount of Pt seed is important for the morphology and distribution of photodeposition Pt cocatalyst. As shown in Fig. S7, the photodeposited Pt particles are aggregated and dense when the amount of Pt seed is 0.04 wt%. The dense Pt cocatalyst will lead to strong light shading effect for Ta_3N_5 photocatalyst and reduced photocatalytic hydrogen evolution rate (Fig. S2a). With a suitable amount of Pt seed (0.01 wt%) impregnated, the Pt(Imp-PD)/Ta_3N_5 shows a dispersive worm-like morphology of Pt cocatalyst, which causes increased contact area between Pt cocatalyst and Ta_3N_5 photocatalyst as well as promoted charge separation and photocatalytic activity.

Encouraged by above finding, we thus extended the metal-seed assistant photodeposition approach into other metal seeds and semiconductors. As seen in Fig. 5, similar promotion on the H_2 evolution rate on the Ta_3N_5 can be observed when either noble (Ru, Rh) or non-noble (Ni, Ag) is employed as seed. As given in Fig. S8, moreover, the H_2 evolution rate on the TaON or $Sr_5Ta_4O_{15\text{-}x}N_x$ photocatalyst can be also promoted by this strategy. The results well demonstrate the generality of our metal-seed assistant photodeposition approach in promoting the photocatalytic activity.

In summary, we report an innovative metal-seed assistant photodeposition approach to exhibit superior H_2 evolution rate from water compared to the conventionally single impregnation or photodeposition process. It has been well demonstrated that remarkably promoted interface charge separation as well as photocatalytic activity can be obtained by the innovative deposition strategy, which is proposed to combine the advantages of impregnation and photodeposition in the interface strong interaction and homogeneous dispersion respectively. Furthermore, our approach shows a good generality and can be easily extended into other systems. Our work may provide an alternative method to fabricate promoted photocatalytic systems.

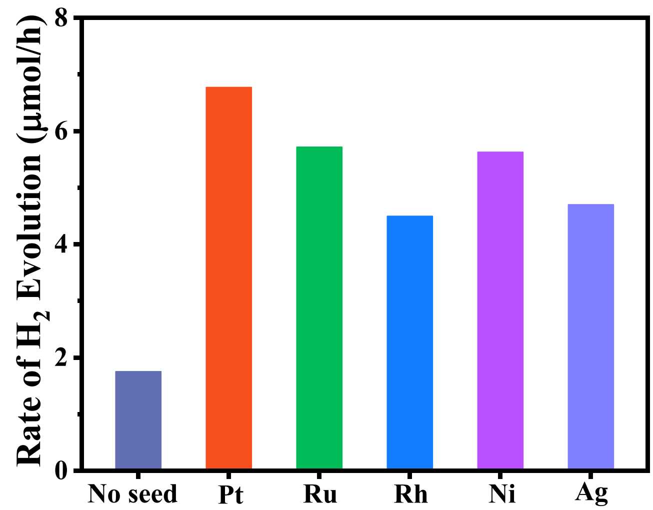

Fig. 5. Rates of H_2 evolution over Pt(Imp-PD)/Ta_3N_5 photocatalysts with no seed or with different metal seeds; the photodeposition Pt cocatalyst is fixed at 1.0 wt%.

Declaration of Competing Interest

The authors declare that they have no known competing financial interests or personal relationships that could have appeared to influence the work reported in this paper.

Acknowledgments

This work was supported by the National Natural Science Foundation of China (21633009, 21925206, 21902156); the Dalian National Laboratory for Clean Energy (DNL) Cooperation Fund, CAS (no. DNL 201913); the International Partnership Program of Chinese Academy of Sciences (121421KYSB20190025) and the DICP foundation of innovative research (DICP I201927). F. Zhang thanks the support from Liao Ning Revitalization Talents Program (XLYC1807241).

Appendix A. Supplementary data

Supplementary data to this article can be found online at https://doi.org/10.1016/j.jechem.2020.07.034.

References

[1] Z. Wang, C. Li, K. Domen, Chem. Soc. Rev. 48 (2019) 2109–2125.
[2] M.M. May, H.J. Lewerenz, D. Lackner, F. Dimroth, T. Hannappel, Nat. Commun. 6 (2015) 8286–8292.

[3] Q. Wang, T. Hisatomi, Q. Jia, H. Tokudome, M. Zhong, C. Wang, Z. Pan, T. Takata, M. Nakabayashi, N. Shibata, Y. Li, I.D. Sharp, A. Kudo, T. Yamada, K. Domen, Nat. Mater. 15 (2016) 611–617.
[4] J. Yang, D. Wang, H. Han, C. Li, Acc. Chem. Res. 46 (2013) 1900–1909.
[5] Z. Zhang, J.T.Y. Jr, Chem. Rev. 112 (2012) 5520–5551.
[6] S. Chen, S. Shen, G. Liu, Y. Qi, F. Zhang, C. Li, Angew. Chem. Int. Ed. Engl. 54 (2015) 3047–3051.
[7] X.T. Xu, L. Pan, X. Zhang, L. Wang, J.J. Zou, Adv. Sci. 6 (2019) 1801505.
[8] S.J.A. Moniz, S.A. Shevlin, D.J. Martin, Z.X. Guo, J. Tang, Energy Environ. Sci. 8 (2015) 731–759.
[9] S. Bai, W. Yin, L. Wang, Z. Li, Y. Xiong, RSC Adv. 6 (2016) 57446–57463.
[10] S. Chen, J. Yang, C. Ding, R. Li, S. Jin, D. Wang, H. Han, F. Zhang, C. Li, J. Mater. Chem. A 1 (2013) 5651–5659.
[11] J. Zhao, X. Wang, Z. Xu, J.S.C. Loo, J. Mater. Chem. A 2 (2014) 15228–15233.
[12] B. Mei, K. Han, G. Mul, ACS Catal. 8 (2018) 9154–9164.
[13] K. Wenderich, K. Han, G. Mul, Part. Part. Syst. Charact. 35 (2018) 1700250.
[14] K. Yamanaka, S. Sato, M. Iwaki, T. Kajino, T. Morikawa, J. Phys. Chem. C 115 (2011) 18348–18353.
[15] G.R. Bamwenda, S. Tsubota, T. Nakamura, M. Haruta, J. Photochem. Photobiol. A 89 (1995) 177–189.
[16] Y.S. Jia, J.X. Yang, D. Zhao, H. Han, C. Li, J. Energy Chem. 23 (2014) 420–426.
[17] K. Maeda, K. Teramura, D. Lu, N. Saito, Y. Inoue, K. Domen, Angew. Chem. 118 (2006) 7970–7973.
[18] K. Wenderich, G. Mul, Chem. Rev. 116 (2016) 14587–14619.
[19] L.P. Wan, F.Q. Xiong, B.X. Zhang, R.X. Che, Y. Li, M.H. Yang, J. Energy Chem. 27 (2018) 367–371.
[20] K. Maeda, R. Abe, K. Domen, J. Phys. Chem. C 115 (2011) 3057–3064.
[21] F. Zhang, J. Chen, X. Zhang, W. Gao, R. Jin, N. Guan, Y. Li, Langmuir 20 (2004) 9329–9334.
[22] L. Zhang, C. Jiang, R. Irfan, S. Tang, X. Chen, P. Du, J. Energy Chem. 30 (2019) 71–77.
[23] S. Chen, Y. Qi, G. Liu, J. Yang, F. Zhang, C. Li, Chem. Commun. 50 (2014) 14415–14417.
[24] G. Hitoki, A. Ishikawa, T. Takata, J.N. Kondo, M. Hara, K. Domen, Chem. Lett. 31 (2002) 736–737.
[25] D. Wang, T. Hisatomi, T. Takata, C. Pan, M. Katayama, J. Kubota, K. Domen, Angew. Chem. Int. Ed. Engl. 52 (2013) 11252–11256.
[26] M. Xiao, B. Luo, M. Lyu, S. Wang, L. Wang, Adv. Energy Mater. 8 (2018) 1701605.
[27] L. Yuliati, J.H. Yang, X. Wang, K. Maeda, T. Takata, M. Antonietti, K. Domen, J. Mater. Chem. 20 (2010) 4295–4298.
[28] M. Xiao, Z. Wang, B. Luo, S. Wang, L. Wang, Appl. Catal. B-Environ. 246 (2019) 195–201.
[29] X. Jiang, X. Fu, L. Zhang, S. Meng, S. Chen, J. Mater. Chem. A 3 (2015) 2271–2282.
[30] S. Liao, J. Shi, C. Ding, M. Liu, F. Xiong, N. Wang, J. Chen, C. Li, J. Energy Chem. 27 (2018) 278–282.
[31] J. Yu, X. Xu, J. Energy Chem. 51 (2020) 30–38.
[32] S.J. Teh, C.W. Lai, S.B.A. Hamid, J. Energy Chem. 25 (2016) 336–344.